University of Puget Sound
Sound Ideas

All Faculty Scholarship

Faculty Scholarship

9-1-2005

Representation Of A Nonspherical Ice Particle By A Collection Of Independent Spheres For Scattering And Absorption Of Radiation: 3. Hollow Columns And Plates

Thomas C. Grenfell
Department of Atmospheric Sciences, University of Washington, Seattle, Washington, USA

Steven P. Neshyba
University of Puget Sound, nesh@pugetsound.edu

Stephen G. Warren
Department of Atmospheric Sciences, University of Washington, Seattle, Washington, USA

Follow this and additional works at: http://soundideas.pugetsound.edu/faculty_pubs

Citation

Representation of a nonspherical ice particle by a collection of independent spheres for scattering and absorption of radiation: 3. Hollow columns and plates

Thomas C. Grenfell

Department of Atmospheric Sciences, University of Washington, Seattle, Washington, USA

Steven P. Neshyba

Department of Chemistry, University of Puget Sound, Tacoma, Washington, USA

Stephen G. Warren

Department of Atmospheric Sciences, University of Washington, Seattle, Washington, USA

[1]   The ability of an assembly of spheres to represent scattering and absorption by a nonspherical ice crystal of the same volume-to-area (V/A) ratio was previously evaluated for convex shapes (circular cylinders and hexagonal prisms). Here we extend the comparison to indented and hollow prisms, which are common in ice clouds. In the equivalent-sphere representation, the crystal mass and surface area are both conserved. Internal surfaces as well as external surfaces contribute to the total surface area; in the model representation both become external surfaces of spheres. The optical depth τ of the model cloud is thus greater than that of the real cloud by the ratio $A/4P$, where A is the total area of the nonspherical particle and P is the orientation-averaged projected area. This ratio, which we call "fluffiness," is unity for convex shapes but may exceed 2 for clusters of hollow bullets. In effect, the scattering at interior surfaces of a hollow crystal becomes classified as multiple scattering in the model of ice spheres. Therefore, rather than directly comparing the asymmetry factor (g) and single-scattering albedo (ω_o) of the hollow crystal to those of the equal-V/A sphere, it is more appropriate to compare the product $\tau(1 - g)\omega_o$, because this quantity largely determines the bulk radiative properties of the cloud. Errors in albedo, absorptance, and transmittance of ice clouds, caused by the equal-V/A representation, are presented for a range of aspect ratios, indentation depths, and ice-water paths at visible and near-infrared wavelengths.

Citation: Grenfell, T. C., S. P. Neshyba, and S. G. Warren (2005), Representation of a nonspherical ice particle by a collection of independent spheres for scattering and absorption of radiation: 3. Hollow columns and plates, *J. Geophys. Res.*, *110*, D17203, doi:10.1029/2005JD005811.

1.   Introduction

[2]   Models to calculate absorption and scattering of light by ice crystals in clouds and snow commonly represent the crystals by "equivalent spheres." This approach typically reduces the computation time for single-scattering quantities by many orders of magnitude compared with exact calculations. Since a great variety of particle shapes occur in ice clouds, in many cases the exact shapes are unknown, so to represent these clouds in climate models and in remote-sensing retrievals it is appropriate to use simpler parameterizations.

[3]   Three choices of equivalent spheres have been used [*Grenfell and Warren*, 1999, Figure 2]. A nonspherical particle may be represented by a sphere of the same volume,

V, or by a sphere of the same surface area, A, or by a collection of spheres with the same volume-to-surface-area ratio, V/A. The equal-volume and equal-area spheres have been shown in many studies [e.g., *Mishchenko et al.*, 2002] to cause large errors. We are instead focusing on the equal-V/A representation, and evaluating its accuracy. The method of equal-V/A spheres is a straightforward technique in which the model cloud conserves both the total mass of ice and the total surface area of particles by adjusting the effective number of particles. Both constraints are important because for weakly absorbing particles, the absorption is proportional to the volume, but the scattering is proportional to the surface area. Matching the number of particles is less important for calculation of the radiation fluxes. In fact, a particular advantage of the equal-V/A representation is that it can be applied unambiguously to a terrestrial snowpack, for example, where the identity of the individual snow particles is in general not well defined.
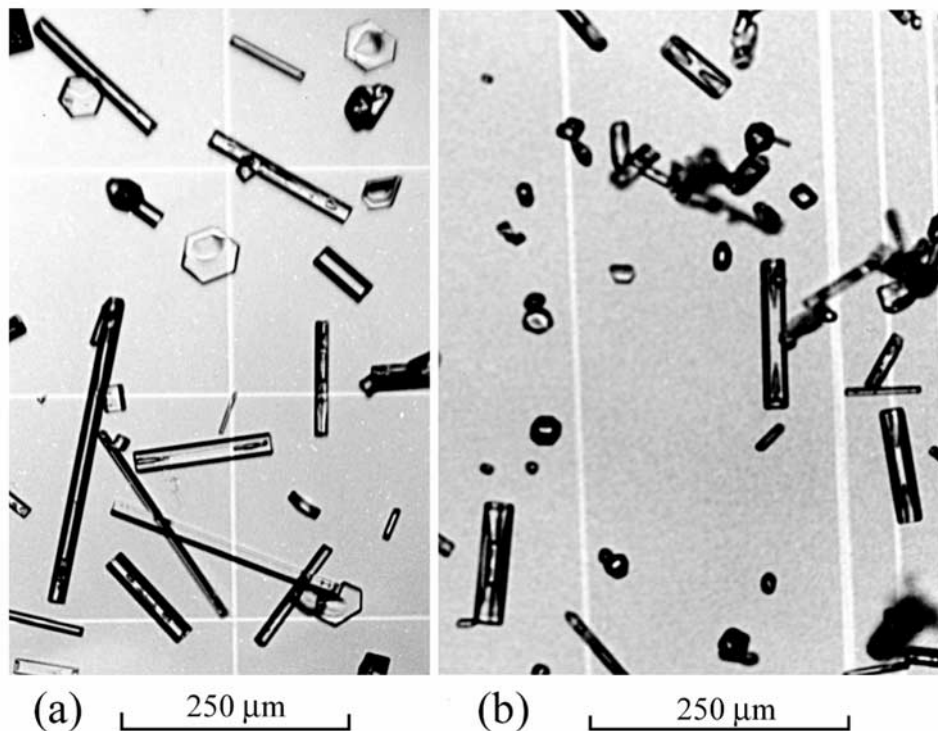
Figure 1. A selection of hollow atmospheric ice crystals collected at South Pole Station as described by *Walden et al.* [2003].

[4] In the first paper of this series, *Grenfell and Warren* [1999] (hereinafter GW99) examined the accuracy of an equal-V/A prescription for randomly oriented infinitely long circular cylinders of ice, surveying a wavelength domain 0.2 to 50 μm over a broad range of cylinder radii and ice-water paths. Subsequently, *Neshyba et al.* [2003] (hereinafter NGW03) extended the study to solid hexagonal ice crystals. In the case of circular cylinders, the equal-V/A sphere prescription did an excellent job of representing the angularly averaged single-scattering and multiple-scattering properties across a broad domain of wavelengths, crystal radii, and cloud thicknesses. The errors in hemispheric reflectance and absorptance rarely exceeded 0.05. For hexagonal columns and plates the errors were likewise small; for equidimensional crystals they were somewhat larger, particularly at visible wavelengths for moderate optical depths.

[5] The application we envision for this parameterization is computation of fluxes for energy budgets. We therefore display the radiative properties of ice clouds only as irradiances. We do not expect the method to be valid for radiances, let alone polarized radiances. However, as pointed out in our first paper [*Grenfell and Warren*, 1999], the concept of equal-V/A spheres is a convenient way to describe the "size" of an ice crystal by a single number, which can be useful in remote sensing as well.

[6] The error survey in this paper builds on an observation made by NGW03, that the asymmetry parameters, g, of equal-V/A spheres exhibit their greatest departures from correct values for an aspect ratio of 1.0 (equidimensional crystals). Using the subscripts s for sphere and x for crystal, $g_s - g_x \approx 0.1$ for equidimensional hexagonal prisms with

equal-V/A radii of 50 μm at a wavelength of 0.5 μm (NGW03, their Figure 7). This "equidimensional aberration" decreases for both larger and smaller aspect ratios (columns and plates respectively). For the example just cited, $g_s - g_x$ switches from positive to negative for hexagonal prisms with aspect ratios of approximately 1/10 (plates) and 10 (columns). Because the equidimensional aberration was observed in the geometric optics limit, it was conjectured by NGW03 that it can be understood in a ray-tracing sense as the result of the relative importance of corner reflectors and parallel faces.

[7] Although solid hexagonal crystals do occur in real ice clouds, it is more common for crystals to contain concavities. Even over the Antarctic Plateau in winter, which is the best place on Earth to find pristine crystals, concavities are common. In the study of *Walden et al.* [2003, Tables 3 and 4], bullet-clusters dominated the volume of falling crystals (i.e., excluding blowing snow), and the individual bullets in those clusters were always hollow. In the future we intend to study clusters of hollow bullets. A selection of simple hollow prisms, the topic of this paper, is shown in Figure 1. Bullet clusters are commonplace in cirrus clouds [e.g., *Ono*, 1969; *Heymsfield*, 1975]; and although the resolution of the available images from those studies was not sufficient to determine how many of the crystals were hollow, we expect to find that hollow crystals do occur in cirrus clouds, and may in fact dominate. The question therefore arises, how well does the equal-V/A sphere formulation fare in approximating the scattering and absorption properties of clouds of such crystals? In this case, by "volume" we mean only the volume occupied by ice, excluding the volume of indentations, hollows, and inclu-
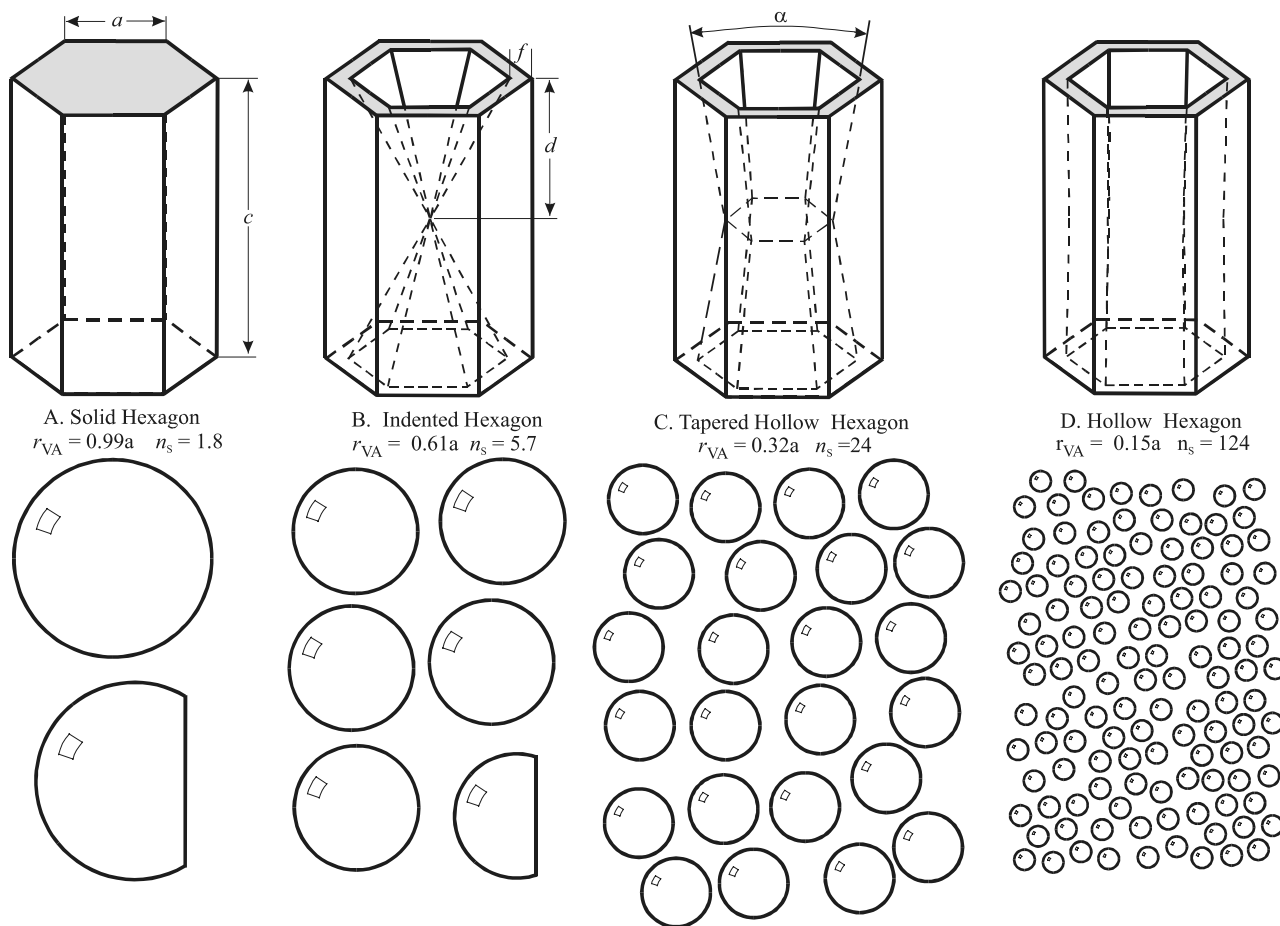
Figure 2. Geometry of the hollow hexagons and associated equal-*V/A* spheres for a given value of the half-width of the basal face, *a*. The crystal length is *c*, the depth of the indentation is *d*, and the basal shoulder width is *f*. In terms of the ratios defined in equations (3)–(5), the crystals shown are specified as follows: (a) $\Gamma = 1.4$, $\Psi = 0$, $\alpha = 180°$; (b) $\Gamma = 1.4$, $\Psi = 1.0$, $\Phi = 0.2$, $\alpha = 60°$; (c) $\Gamma = 1.4$, $\Psi = 3.0$, $\Phi = 0.2$, $\alpha = 20°$; and (d) $\Gamma = 1.4$, $\Psi = 100$, $\Phi = 0.2$, $\alpha \approx 0°$, where α is the opening angle as shown in Figure 2c. The corresponding size and number of equal-*V/A* spheres are given below each crystal. The opening angle, α, is given by $\alpha = 2 \tan^{-1}[(1 - \Phi)/(\Gamma\Psi)]$.

sions. Of particular interest is the effect of variations of the asymmetry parameter in conjunction with the degree of hollowing, and the effect of the internal surface area on the model's optical depth.

[8] Our computational approach is to use a ray-tracing algorithm for single scattering, followed by a four-stream delta-M discrete-ordinates radiative transfer model to calculate the radiation fluxes associated with plane-parallel clouds made up of such particles. On the basis of the analysis of *Yang and Liou* [1997] for hexagonal crystals, ray tracing calculations produce sufficiently accurate results for a size parameter associated with the small dimension of about 50 or greater. The corresponding size parameters in this study are ≥80. Ray tracing calculations are computationally much faster than exact formulations such as the FDTD [*Yang and Liou*, 1996] and T-Matrix [*Havemann and Baran*, 2001] methods, and the greater computational efficiency has allowed us to explore a wide assortment of shape parameters associated with such particles.

[9] Figure 2 shows schematic diagrams of hollow hexagonal prisms and the corresponding equivalent spheres, and defines the shape parameters that specify the prisms included in this study. The prisms have identical hexagonal indentations opening at both ends. As in our previous work, *a* and *c* specify the half-width of the basal face (a-axis dimension) and the length (c-axis dimension) respectively. Γ is the exterior aspect ratio, *c/2a*. Parameter Φ specifies the wall thickness at the end of the prism: $\Phi = 0$ corresponds to zero thickness at the opening, while $\Phi = 1$ corresponds to walls with maximum thickness (a solid hexagon). The indentation of the crystal is defined by the depth *d*, but it is useful to describe it by the ratio $\Psi = 2d/c$, which ranges from zero for solid hexagons to infinity for hexagons with a hexagonal hole aligned with the c-axis whose walls are parallel to the outside surfaces. Easier to visualize is the angle subtended by opposing faces of the indentation, defined here as $\alpha = 2 \tan^{-1}[(1 - \Phi)/(\Gamma\Psi)]$. For limiting values of Ψ, this opening angle depends only on Ψ: no indentation ($\Psi = 0$) corresponds to $\alpha = 180°$, while maximum indentation ($\Psi = \infty$) corresponds to $\alpha = 0°$. For intermediate values of Ψ, the value of α also depends on the aspect ratio and the wall thickness. For example for

Figure 2b, $\Psi = 1$, $\Phi = 0.2$, and $\Gamma = 1.4$ correspond to an opening angle $\alpha = 60°$.

2. Equivalent-Sphere Representation for Hollow Crystals

[10] Following GW99 and NGW03, we represent a particle of volume V and surface area A by a collection of spheres that preserves both V and A. Since the ratio V/A for a sphere equals $r/3$, the required radius of the equal-V/A sphere is

$$r_{VA} = 3\frac{V}{A}, \tag{1}$$

and the number of equivalent spheres per nonspherical particle, n_s, is given by

$$n_s = \frac{3\,V}{4\,\pi\,r_{VA}^3}. \tag{2}$$

These two formulae can be readily applied to concave hexagonal crystals as shown in Figure 2. As in NGW03, we define the aspect ratio, Γ, for hexagonal crystals,

$$\Gamma = \frac{c}{2\,a}. \tag{3}$$

For hollow crystals we define two additional ratios,

$$\Psi = \frac{2\,d}{c}, \tag{4}$$

$$\Phi = \frac{f}{a}, \tag{5}$$

where the dimensions a, c, d, and f are shown in Figure 2. The geometry of the crystals can then be specified using these dimensionless ratios and a single linear dimension, for example a, by noting that

$$c = 2\,a\,\Gamma,$$

$$d = a\,\Gamma\,\Psi, \tag{6a}$$

$$f = a\,\Phi.$$

To distinguish among the cases for which the indentation produces a hole through the center of the crystal we also define

$$Y = 1 \text{ if } \Psi < 1 \text{ (no hole)}$$
$$\tag{6b}$$
$$Y = \Psi \text{ if } \Psi \geq 1 \text{ (hole)}.$$

The radii of the equal-V/A spheres are given by

$$r_{VA} = a \cdot \frac{\sqrt{3}\,\Gamma\left[3 - (1-\Phi)^2\Psi\left[1 - \left(1 - \frac{1}{Y}\right)^3\right]\right]}{4\,\Gamma + \sqrt{3}\,\Phi\,(2-\Phi) + (1-\Phi)\sqrt{3\,(1-\Phi)^2 + 4\,(\Gamma\Psi)^2\left[1 - \left(1 - \frac{1}{Y}\right)^2\right]}}. \tag{7}$$

The number of spheres per crystal is then determined from equation (2) using (7) together with the volume of ice in the crystal,

$$V_x = \sqrt{3}\,a^3\,\Gamma\left[3 - (1-\Phi)^2\Psi\left[1 - \left(1 - \frac{1}{Y}\right)^3\right]\right]. \tag{8}$$

Note that n_s depends only on the ratios defined in equations (3)–(5) and not on the size of the crystals. In the limit that the indentation disappears ($\Psi \to 0$), we have

$$\lim_{\Psi \to 0} V_x = 3\sqrt{3}\,a^3\,\Gamma \tag{9a}$$

$$\lim_{\Psi \to 0} r_{VA} = a\frac{3\sqrt{3}\,\Gamma}{4\,\Gamma + \sqrt{3}}. \tag{9b}$$

These are identical to the values for solid hexagons (NWG03, equations (6c) and (3)). In the opposite limit $\Psi \to \infty$), we consider a polynomial expansion of $(1 - \frac{1}{\Psi})^n$ noting that in the limit of large Ψ,

$$\lim_{\Psi \to \infty}\left(1 - \frac{1}{\Psi}\right)^n = \left(1 - \frac{n}{\Psi}\right),$$

and we obtain

$$\lim_{\Psi \to \infty} V_x = 3\sqrt{3}\,a^3\,\Gamma - 3\sqrt{3}(1-\Phi)^2\,a^3\,\Gamma. \tag{10a}$$

Since $c = 2a\Gamma$, and $a(1 - \Phi)$ is the distance from the center of the crystal to the inside wall, a brief calculation shows that in this limit V_x is the volume of the hexagonal outer shell minus the volume of the hexagonal void inside it, as expected.

[11] The surface area in the limit $\Psi \to \infty$ is equal to the area of a hexagon with a nested hexagonal hole through the c-axis, $\lim_{\Psi \to \infty} A_x = 6ac + 3\sqrt{3}\,[a^2 - (a - f)^2] + 6\,(a - f)c$. The limit for r_{VA} is then

$$\lim_{\Psi \to \infty} r_{VA} = 3\,\lim_{\Psi \to \infty}\left(\frac{V_x}{A_x}\right), \tag{10b}$$

consistent with equation (1). Further, as Φ approaches 1, we find that as the hole vanishes,

$$\lim_{\Phi \to 1}\lim_{\Psi \to \infty} r_{VA} = a \cdot \frac{3\sqrt{3}\,\Gamma}{4\,\Gamma + \sqrt{3}}, \tag{10c}$$

recovering NGW03 equation (6a).

3. Single Scattering

[12] The first stage is to calculate the single scattering properties of the particles to be compared. For each non-spherical particle we consider the scattering properties averaged over orientation for a randomly oriented ensemble. For spheres, we average over a lognormal size distribution to smooth out resonance features. The distribution is chosen such that the effective radius (NGW03 equation (11), for
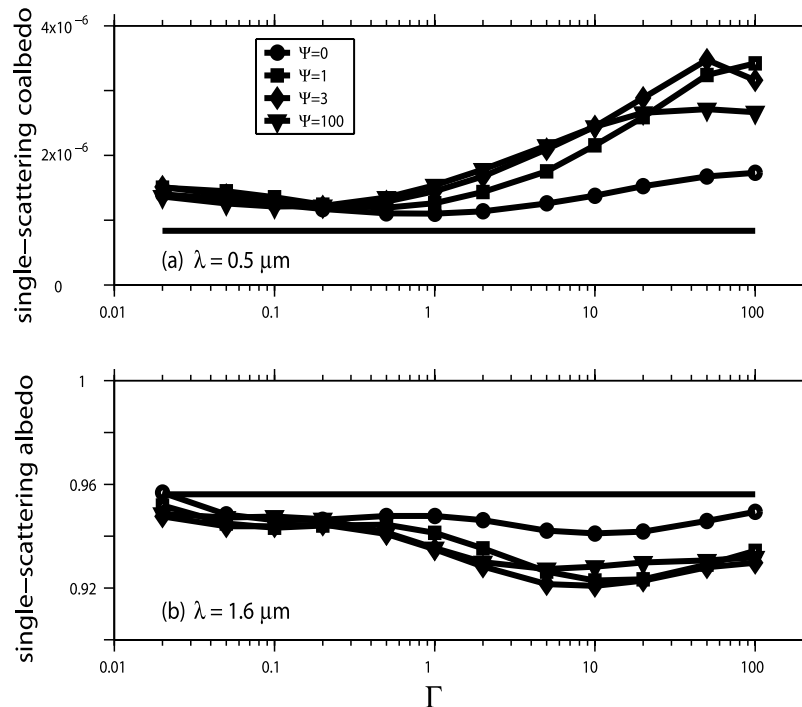
Figure 3. (a) Single-scattering coalbedo, $(1 - \omega_o)$, as a function of aspect ratio for concave ice crystals for a range of indentation parameters Ψ at a wavelength of $\lambda = 0.5 \ \mu m$. (b) Single-scattering albedo at $\lambda = 1.6 \ \mu m$. The horizontal lines indicate the values for equal-V/A spheres. In both panels, $\Phi = 0.2$ and $r_{VA} = 20 \ \mu m$.

example) is equal to r_{VA} for the non-spherical particle in question.

3.1. Mie Theory and Ray Tracing

[13] The scattering properties of spheres were calculated from Mie theory, using the computer code of *Wiscombe* [1979, 1980]. For randomly oriented concave hexagonal crystals a ray-tracing code supplied by A. Macke was employed [*Macke et al.*, 1996]. In this implementation, a "ray" of electromagnetic radiation is defined by a direction of propagation, direction of electric field vectors, and a Stokes vector, although here we consider only unpolarized radiation since we are interested only in radiation fluxes. The algorithm addresses reflection and transmission of a bundle of parallel rays by ice polyhedra. For each crystal orientation, the diffraction component is calculated from the geometrical cross section. Legendre moments of the phase function (of which the first is the asymmetry parameter, g) are calculated by numerical integration. For the calculations, we specified 100 rays per crystal orientation, with a maximum of 100 total internal reflections. Ten thousand orientations were calculated for each crystal shape. We compared selected cases of 100 rays and 10,000 orientations with more accurate computations using 300 rays and 30,000 orientations. The differences were sufficiently small that we decided to use 100 rays and 10,000 orientations for the complete set of analyses.

[14] Because of the large number of variables needed to describe the hollow crystals, we limit the results to only two wavelengths, 0.5 μm and 1.6 μm. These provide cases with very small absorption and moderate absorption respectively, and are cases where we had found the largest errors in our

prior analysis (NWG03). It would be interesting also to examine a case of strong absorption in the thermal infrared, for example, $\lambda = 11 \ \mu m$, but the crystal sizes found in cirrus are not in the geometric-optics limit for that wavelength.

3.2. Results for Single Scattering

[15] Figure 3 displays single-scattering albedo ω_o (or single-scattering coalbedo, $1 - \omega_o$) as a function of Γ for varying indentation parameters (Ψ), at the visible and near-infrared wavelengths. The single-scattering albedo of equal-V/A spheres is higher than that of the crystals over most of the range. The discrepancy is smaller for solid hexagonal ice crystals ($\Psi = 0$) than for the hollow ones. However, we will show below in section 3.4 that for concave crystals it is misleading to compare values of ω_o directly. Instead a combination of ω_o, g, and τ is relevant.

[16] Figure 4 displays the asymmetry parameter as a function of Γ, for varying indentation parameters, at the two wavelengths. Note the dip below the equal-V/A sphere value for solid equidimensional hexagonal ice crystals, with a minimum at $\Gamma \approx 1$, as in Figure 7 of NGW03. The minimum becomes less pronounced and shifts to smaller values of Γ for concave crystals with increasing indentations. This figure covers a very wide range of Γ. Plates and columns found in the atmosphere are likely to have Γ values limited to a more restricted range, from 0.1 to 30, as will be illustrated in Figure 10 in section 4.2.

3.3. Transformation of Optical Depth by "Fluffiness"

[17] When a hollow crystal is represented by a collection of equal-V/A spheres, the interior surfaces of the crystal are represented as exterior surfaces of spheres. Consequently
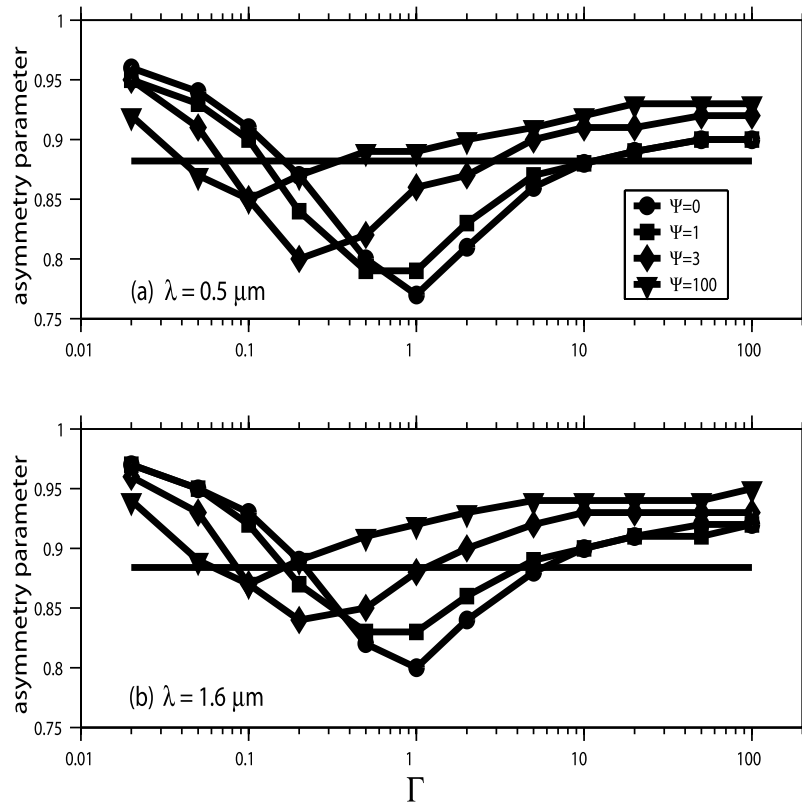
Figure 4. As in Figure 3, but showing the asymmetry parameter, (a) for $\lambda = 0.5$ μm, and (b) for $\lambda = 1.6$ μm.

the total projected area of the spheres exceeds the projected area of the crystal, and the optical depth of the model cloud, τ_s, exceeds that of the real cloud, τ_x. Physically what is happening is that the interior surfaces of a crystal can cause a photon to scatter several times within a crystal before exiting. In some cases this may result in less forward scattering, more side scattering and backscattering, and a low value for g_x. In the spherical representation, this scattering at the interior surfaces of an ice crystal becomes classified as multiple scattering, resulting in an adjusted optical depth.

[18] The ratio of surface area, A, to orientationally averaged projected area, P, is exactly 4 for a sphere or for any convex three-dimensional shape [*Vouk*, 1948]. For a crystal containing concavities, A/P exceeds 4. The optical depth of the model cloud of spheres, τ_s, relative to the optical depth of the real cloud, τ_x, is derived from equations (1), (2) and (8) of GW99,

$$\frac{\tau_s}{\tau_x} = \frac{A}{4P} \frac{Q_{ext,s}}{Q_{ext,x}}, \tag{11}$$

where P is the orientation-averaged projected area for the crystals. It is convenient to define the "fluffiness," F, of a particle as

$$F = \frac{A}{4P}, \tag{12}$$

For convex particles $F = 1$, but for concave particles with excess area associated with interior surfaces, we have in general that $F > 1$; and F tends to increase with degree of hollowing and complexity in crystal shape.

[19] For crystals and spheres that are both large enough that $Q_{ext} \approx 2$, we see from equations (11) and (12) that the ratio of optical depth of the model cloud to optical depth of the real cloud is equal to the fluffiness,

$$\frac{\tau_s}{\tau_x} = F. \tag{13}$$

3.4. Similarity-Parameter Ratio

[20] Since our objective is to assess the accuracy of equal-V/A spheres for determining radiative energy fluxes, we note that it is necessary to consider more than just the significant differences in asymmetry parameter. In particular, the effects of single scattering albedo and variations in optical depth must also be taken into account. This is done consistently in our multiple scattering calculations, described below; however, we can formulate a predictive criterion by making use of the concept of the similarity principle, which has been considered in some detail by *van de Hulst* [1980, chap. 14] and *Liou* [2000, sect. 6.5.3].

[21] The similarity principle seeks to define a similarity parameter, $S = S(Q_{ext}, \omega_o, g)$, such that the apparent optical properties of a multiple-scattering medium do not differ much for combinations of its arguments that leave S invariant. Our objective is to find an S suitable for comparing spheres and crystal forms. Various possibilities have been discussed depending on particular restrictions imposed on the optical depth and on the various radiation fluxes. We
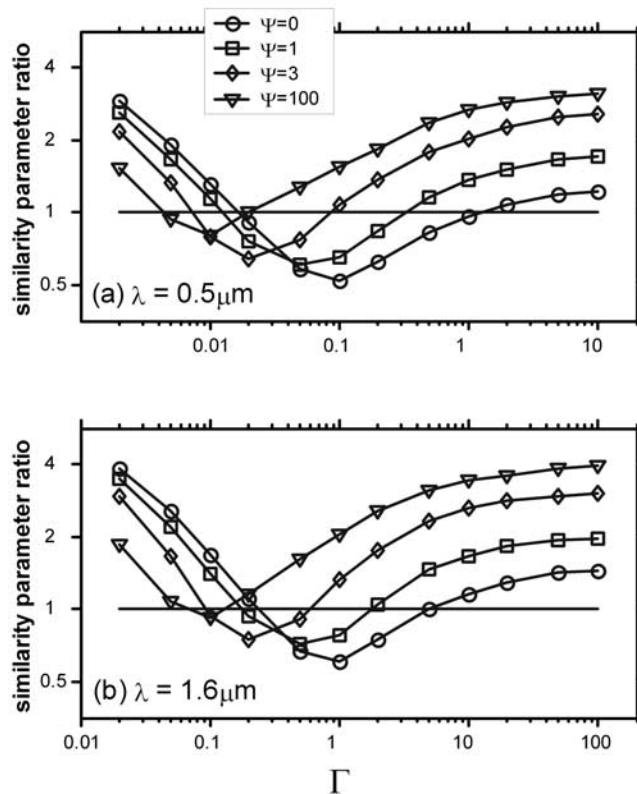
Figure 5. As in Figure 3, but showing the ratio of similarity parameters (equation (16)), (a) for λ = 0.5 μm, and (b) for λ = 1.6 μm; the horizontal lines indicate ratios at which the equal-V/A sphere representation is expected to be most accurate.

tested several of these and found a form of particular utility that is derived as follows. Starting with Liou's equation (6.5.36a), we require that

$$\tau_x(1 - g_x)\omega_{o,x} = \tau_s(1 - g_s)\omega_{o,s}. \qquad (14)$$

This requirement is derived from the delta-M transformation, which was designed to preserve the total attenuation of diffuse radiation by the medium and to adjust for differences in ω_o and g such that the mathematical form and the solution of the equation of transfer are preserved. Equation (14) is also consistent with a theoretical result of the two-stream method [e.g., *Coakley and Chylek*, 1975] that the albedo and transmittance of a nonabsorbing cloud (ω_o = 1) are determined by the product $\tau(1 - g)$.

[22] Combining equations (11), (12), and (14), we define the similarity parameter for particle type p,

$$S_p = \frac{(1 - g_p)\,\omega_{o,p}}{F_p}, \qquad (15)$$

and we define the similarity ratio, R, as the ratio of similarity parameters for sphere (for which fluffiness equals one) and crystal (with fluffiness $F \geq 1$),

$$R = \frac{\tau_s}{\tau_x}\frac{(1 - g_s)\omega_{o,s}}{(1 - g_x)\omega_{o,x}} = F\frac{(1 - g_s)\omega_{o,s}}{(1 - g_x)\omega_{o,x}} \qquad (16)$$

[23] The ratio R provides a quantitative index to investigate the applicability of the similarity principle. If S is nearly the same for crystals and spheres, then $R \approx 1$, and we expect that the model of equivalent spheres will give accurate results in multiple-scattering. For complex ice crystals with concavities, measurements in Arctic clouds [*Gerber et al.*, 2000] have found an average g_x of 0.74. Since $g_s \approx 0.87$ for the equal-V/A spheres, we would expect the altered τ in the model to compensate for the altered g, yielding $R \approx 1$ if $F \approx 2$. *Schmitt and Heymsfield* [2005] have developed a method to estimate internal surface areas from images of ice particles. For particle populations in tropical cirrus clouds, they do find fluffiness values of 2.0 to 2.5. The shapes in Figures 2c and 2d (Ψ = 3 and 100) also have fluffiness values approaching 2, but Figure 4 shows that the expected compensation of τ and g does not occur in these cases. None of our hollow crystals have asymmetry parameters as low as those observed by Gerber et al., and in fact the g_x values of our crystals actually exceed g_s for most aspect ratios. We will proceed with the computation of multiple-scattering errors for the shapes shown in Figure 2, but the above discussion suggests that the equivalent-sphere representation may work much better for real clouds with $g_x \approx 0.74$ than for the shapes considered here, where g_x often exceeds 0.9.

[24] Figure 5 displays R as a function of Γ for varying crystal indentations, Ψ, at our visible and infrared wavelengths. R varies considerably, from about 0.5 to 3.2 at the visible wavelength, and from 0.7 to 4.0 at 1.6 μm. For each indentation Ψ, there are two values of Γ for which $R = 1$. As in the case of asymmetry parameters (Figure 4), the minimum in R becomes less pronounced and shifts to smaller values of Γ for concave crystals with increasingly thin walls. The extent to which a value of $R \approx 1$ is a good indicator of multiple-scattering success for the equal-V/A spheres will be evaluated in section 5.

4. Multiple Scattering

[25] We now compare the bulk radiative properties of a horizontally homogeneous cloud of randomly oriented hexagonal ice prisms to those of a cloud of equal-V/A spheres. Calculations of the apparent optical properties (hemispherical reflectance, absorptance, and transmittance) are carried out for a cloud consisting only of ice crystals, for wavelengths of 0.5 and 1.6 μm using a four-stream delta-M discrete-ordinates program [*Grenfell*, 1991]. To isolate the optical properties of the cloud itself, the model consists of a single homogeneous plane-parallel cloud layer over a black surface, illuminated from above by a plane wave at the global average solar zenith angle of 60°. We plot the apparent optical properties as functions of the ice water path (IWP), defined as the total mass per unit area, integrated vertically through the cloud.

4.1. Monodisperse Crystals

[26] For randomly oriented hollow crystals of the same size and shape, the relation of IWP to cloud optical depth, τ_x, is found to be

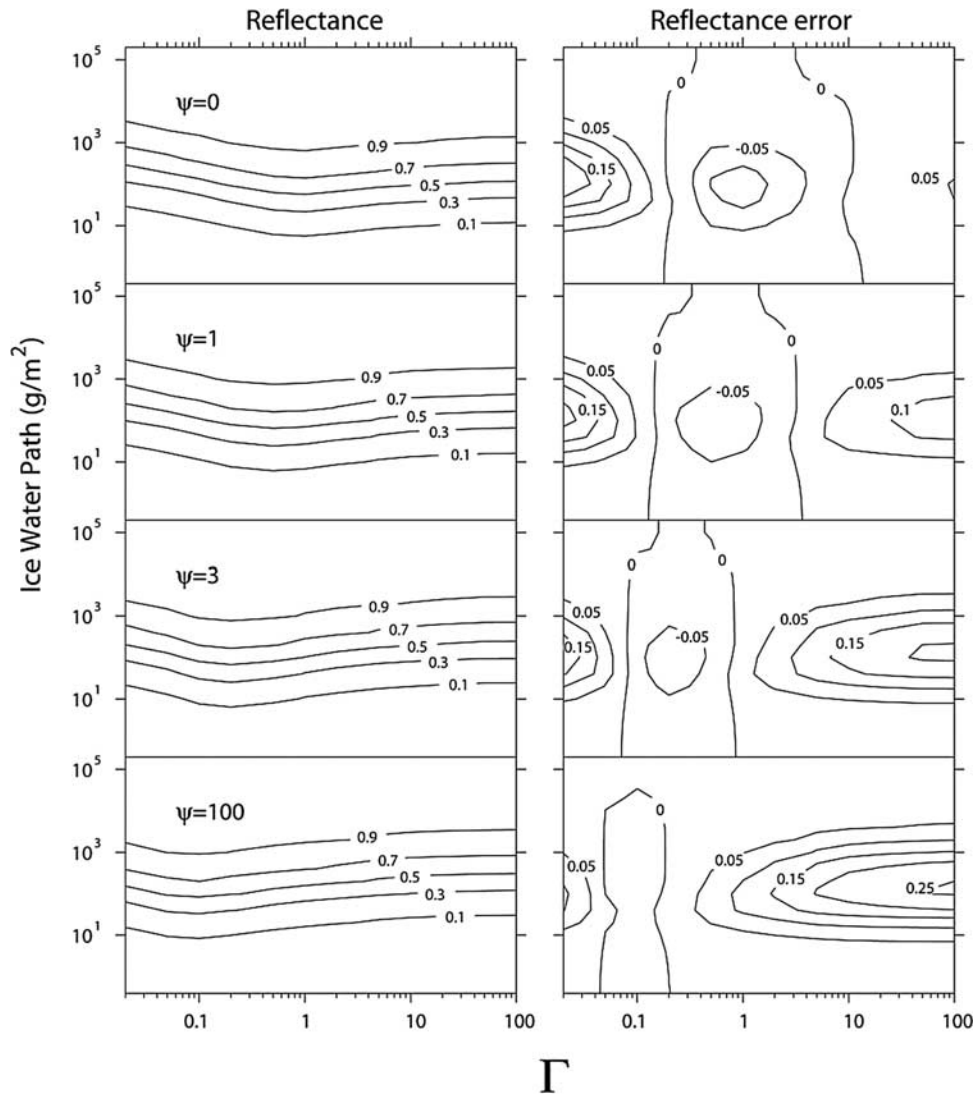$$\tau_x = \frac{3}{4}\frac{\mathrm{IWP}\,Q_{ext}}{r_{VA}\,\rho_{ice}}\frac{1}{F}, \qquad (17)$$

Figure 6. Contours of reflectance and reflectance error, for clouds consisting of concave ice crystals, as functions of ice-water path and aspect ratio at $\lambda = 0.5\mu m$, $r_{VA} = 20$ µm and $\Phi = 0.2$. Results for four indentations are shown. The plotted error is the reflectance using spheres minus the true reflectance.

where ρ_{ice} is the density of pure ice, 917 kg/m^3. (In the case $F = 1$ (no concavities), this equation is identical to NGW03 equation (15).) The generalization of NGW03's equation (16) is, from equations (11) and (12) above,

$$\frac{\tau_s}{\tau_x} = \frac{Q_{ext,s}}{Q_{ext,x}}\text{F.} \qquad (18)$$

[27] Figures 6–9 show the values of cloud reflectance, absorptance, and transmittance for the wavelengths 0.5 and 1.6 µm, as well as the corresponding errors; that is, the differences between the equivalent-sphere results and the exact solution. Reflectance (albedo), r, is defined as the ratio of upwelling irradiance above the cloud to the incident irradiance. Absorptance, a, and transmittance, t, are ratios of absorbed and transmitted irradiance to incident irradiance. The results are displayed as contour plots as a

function of crystal aspect ratio and IWP for Ψ values of 0, 1, 3, and 100.

[28] At $\lambda = 0.5$ µm we plot only the reflectance results (Figure 6), since the absorptance is very small and $t = (1 - r)$ to high accuracy. In this case, reflectance is a relatively weak function of Γ and increases from near zero for the smallest IWP values to 1.0 for IWP $\approx 10^5$. The reflectance error is larger for the hollow crystals than for solid crystals ($\Psi = 0$); the error in representing hollow crystals is largest for extreme shapes (long columns or thin plates) and smaller for equidimensional crystals. In fact, the large errors on the left and right sides of Figures 6–9 are probably not important for atmospheric applications, because atmospheric ice crystals appear to have aspect ratios mostly in the range 0.1–30 where the errors are much smaller.

[29] For $\lambda = 1.6$ µm, absorptance is not negligible, so reflectance, absorptance, and transmittance are all presented
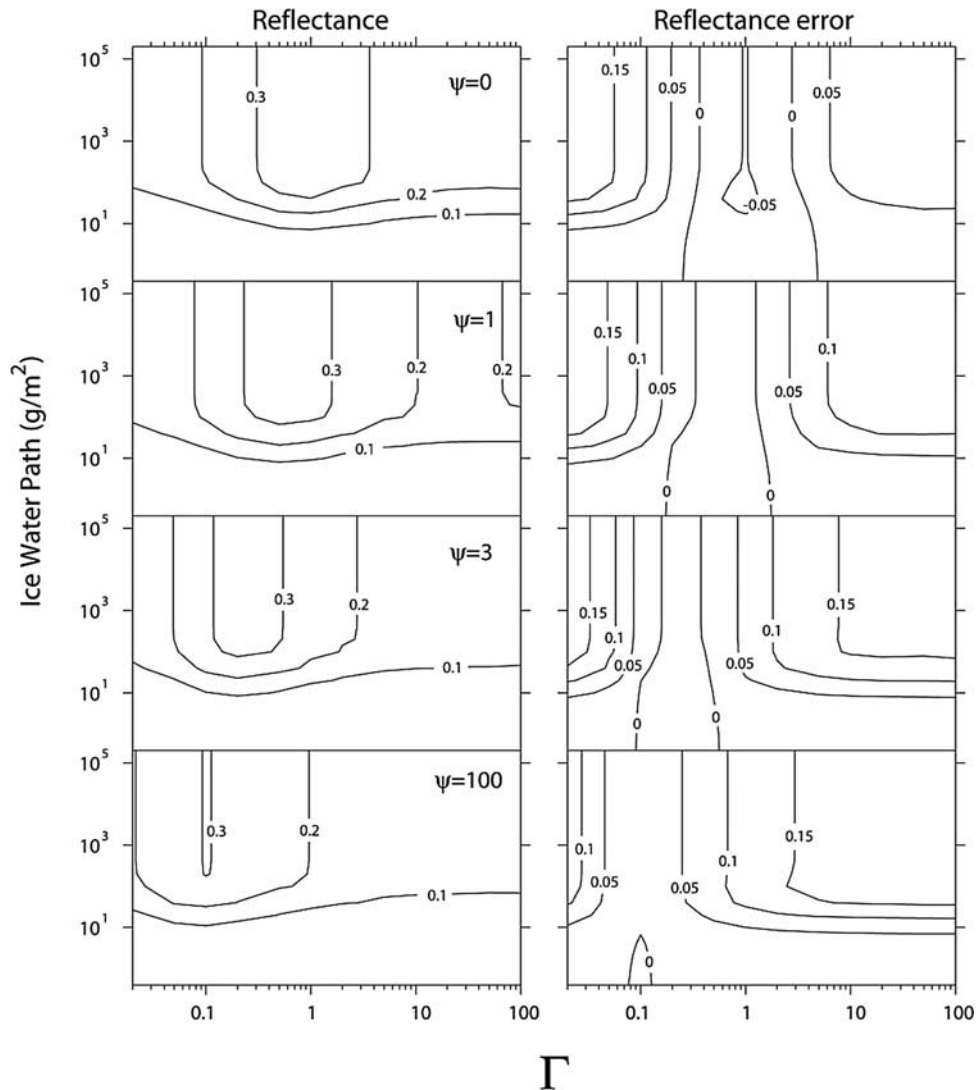
Figure 7. Reflectance and reflectance error for λ = 1.6 μm, r_{VA} = 20 μm and Φ = 0.2.

in Figures 7 through 9. The transmittance error shows behavior similar to the visible reflectance error (Figure 6) in its dependence on Γ. For IWPs exceeding 20–30 g m^{-2}, the transmittance is very small and the reflectance and absorptance patterns are conjugates of one another; i.e., $a = 1 - r$, and $\Delta a = -\Delta r$, where Δ means error. In this region, r and a depend strongly on Γ but are nearly independent of IWP. Still the errors are below 0.05 over a band of Γ values that depends on Ψ (0.2–7, 1.6–2.5, 0.07–1, and 0.05–0.26 respectively, for Ψ values 0, 1, 3, and 100). As was true for the visible wavelength, the largest errors are for extreme shapes, and the widest band of small error is for the solid columns. (For values of IWP below about 10 g m^{-2}, the Γ-dependence is weak for all three quantities, and the errors are all less than 0.05.)

4.2. Clouds With a Distribution of Aspect Ratios

[30] The errors shown in Figures 6–9 are for monodispersions. The errors in representing real clouds may be smaller, because the spread of aspect ratios, indentations, and crystal sizes in a real cloud will include domains of both positive and negative error. We investigate this possibility using the shape distribution presented by *Walden et al.* [2003] for atmospheric ice crystals collected at South Pole Station during 100 days in the winter of 1992. For this work we exclude blowing snow and clusters, and consider only the shape-distributions of simple prisms such as shown in Figure 1, for which 4508 crystals were measured [*Walden et al.*, 2003, Figure 4]. To apply the present technique to this data set we extend the calculation of cloud optical depth and fluffiness to a polydispersion over Γ with a distribution function $N(\Gamma)$. From a straightforward generalization of GW99's equation (11), we have for the crystals

$$\tau_x = \frac{\text{IWP}}{\rho_{ice}} \frac{\displaystyle\int_{\Gamma_{min}}^{\Gamma_{max}} \langle P(\Gamma) \rangle \, N(\Gamma) \, Q_{ext,x}(\Gamma) \, d\Gamma}{\displaystyle\int_{\Gamma_{min}}^{\Gamma_{max}} V_x(\Gamma) \, N(\Gamma) \, d\Gamma}, \tag{19}$$
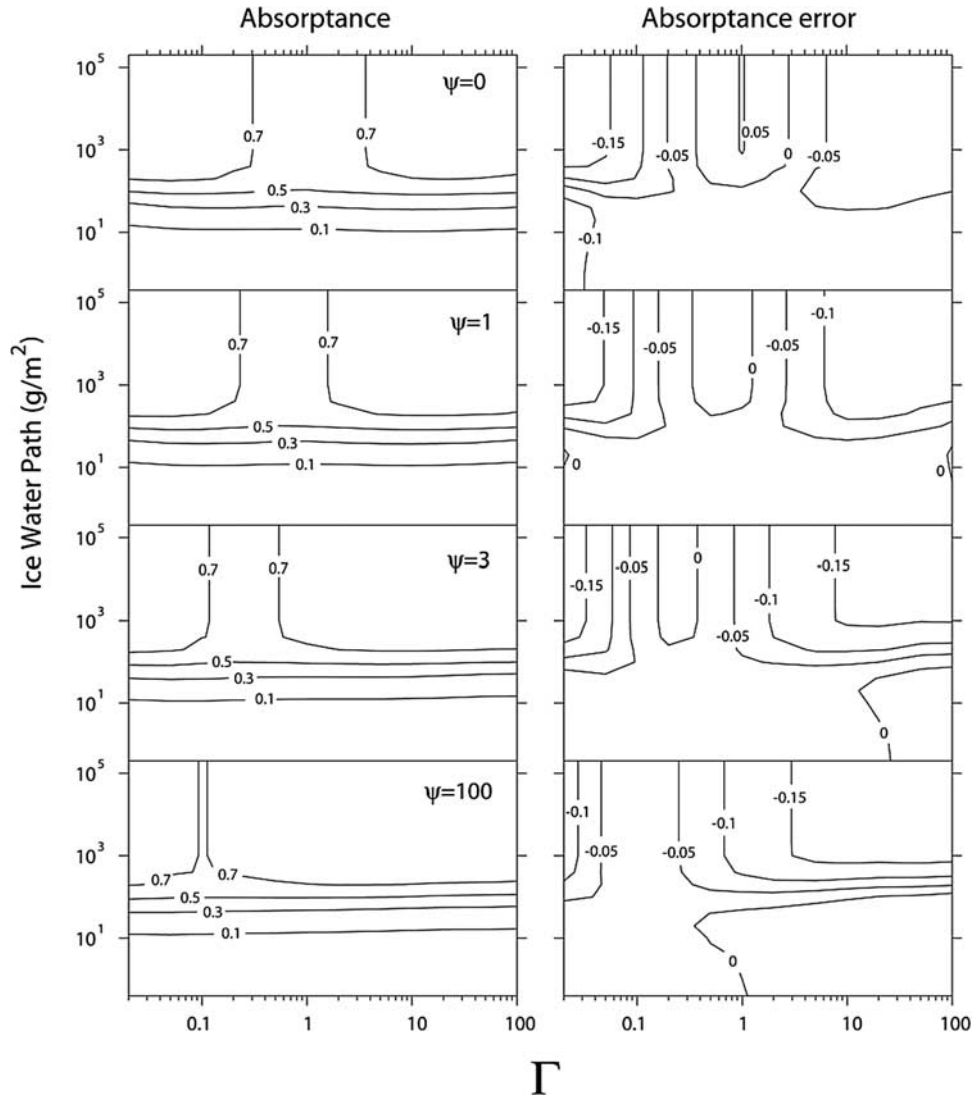
Figure 8. Absorptance and absorptance error for $\lambda = 1.6 \ \mu m$, $r_{VA} = 20 \ \mu m$ and $\Phi = 0.2$.

This can be expressed in a form analogous to GW99 equation (12),

$$\tau_x = \frac{3}{4} \frac{\text{IWP} \ Q_{ext\_eff}}{r_{VA\_eff} \ \rho_{ice}} \frac{1}{F_{eff}}, \tag{20}$$

where the effective quantities are given by

$$Q_{ext,eff} = \frac{\displaystyle\int_{\Gamma_{min}}^{\Gamma_{max}} \langle P(\Gamma) \rangle \ N(\Gamma) \ Q_{ext,x}(\Gamma) \ d\Gamma}{\displaystyle\int_{\Gamma_{min}}^{\Gamma_{max}} \langle P(\Gamma) \rangle \ N(\Gamma) \ d\Gamma}, \tag{21}$$

$$F_{eff} = \frac{\displaystyle\int_{\Gamma_{min}}^{\Gamma_{max}} A_x(\Gamma) \ N(\Gamma) \ d\Gamma}{\displaystyle\int_{\Gamma_{min}}^{\Gamma_{max}} 4 \langle P(\Gamma) \rangle \ N(\Gamma) \ d\Gamma}, \tag{22}$$

$$r_{VA,eff} = 3 \frac{V_{x,eff}}{A_{x,eff}}, \tag{23}$$

where

$$V_{x,eff} = \frac{\displaystyle\int_{\Gamma_{min}}^{\Gamma_{max}} V_x(\Gamma) \ N(\Gamma) \ d\Gamma}{\displaystyle\int_{\Gamma_{min}}^{\Gamma_{max}} N(\Gamma) \ d\Gamma} \tag{24}$$

$$A_{x,eff} = \frac{\displaystyle\int_{\Gamma_{min}}^{\Gamma_{max}} A_x(\Gamma) \ N(\Gamma) \ d\Gamma}{\displaystyle\int_{\Gamma_{min}}^{\Gamma_{max}} N(\Gamma) \ d\Gamma}. \tag{25}$$

[31] The crystal shape distribution (Figure 10) is bimodal, and can be represented as a sum of two lognormal Gaussian
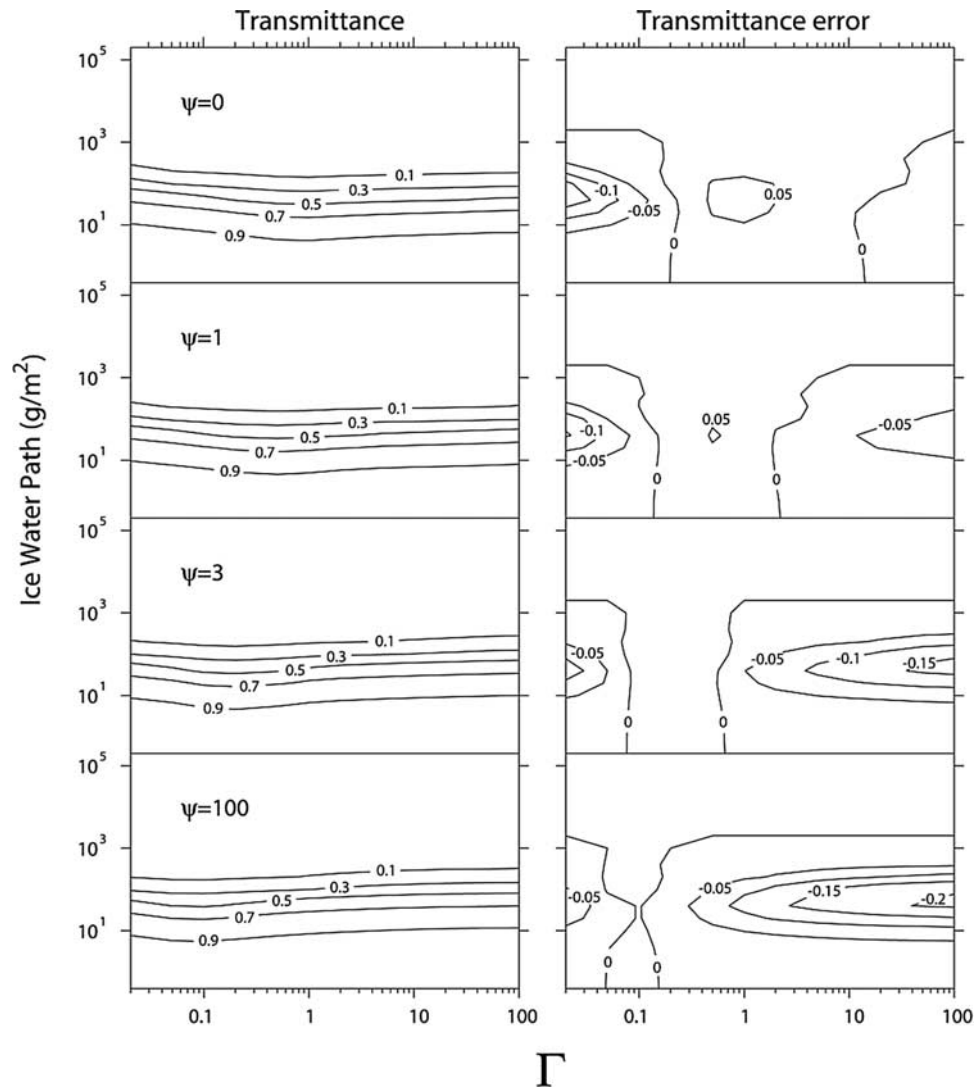
Figure 9. Transmittance and transmittance error for $\lambda = 1.6$ μm, $r_{VA} = 20$ μm and $\Phi = 0.2$.

functions with geometric mean values $\Gamma_g = 0.5$ and 3, and geometric standard deviations $\sigma_g = 0.18$ and 0.34, corresponding to plates and columns, respectively. Note that the minimum between the two modes occurs very close to $\Gamma = 1$, equidimensional prisms. This puts a reduced weight on the range of Γ values where equal-V/A spheres produce large errors for the solid prisms (NGW03).

[32] The results of the multiple scattering calculations at 0.5 and 1.6 μm are shown in Figure 11 for each of the two modes individually as well as for the combination of the two. We show reflectance and absorptance for clouds of equal-V/A spheres, compared to solid prisms and also to hollow prisms with $\Psi = 1$, all of which have $r_{VA} = 20$ μm. The indentation $\Psi = 1$ was chosen based on visual inspection of the hollowed crystals in Figure 1. Both reflectance and absorptance increase smoothly with IWP, reaching saturated values at about 10^4 and 10^2 g m^{-2} at $\lambda = 0.5$ μm and 1.6 μm respectively. For the column mode, the errors in the spherical representation at 1.6 μm for both reflectance and absorptance are less than about 0.05 for the solid columns and 0.07 for the hollow crystals. For the plate

mode, the equivalent sphere results agree within 0.09 at 0.5 μm and within 0.03 at 1.6 μm for both crystal types. For the combined case, the errors are intermediate with a maximum of about 0.06 at 0.5 μm for solid crystals. Slightly better overall agreement is obtained for solid crystals than for hollow crystals.

5. Discussion

[33] To test the utility of the similarity ratio for predicting accuracy of irradiance calculations, we show in Figure 12 the errors in the multiple-scattering results as a function of the similarity-parameter ratio R (equation (16)), covering the full ranges of Γ and IWP for selected values of indentation Ψ and shoulder-width Φ. Results are displayed for a solid prism and a hollow prism, as examples of a general pattern. The errors lie in two opposed fan-shaped domains with a narrow neck near $R = 1$, and they span a range from zero to a maximum value for which optical depth $\tau \sim 1$. At any given value of R, the range of errors displayed is due to various values of optical depth.
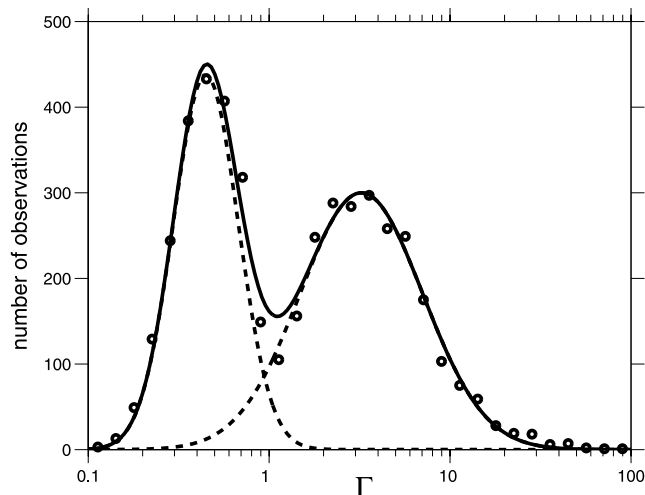
Figure 10. Frequency distribution of aspect ratios for atmospheric ice crystals observed at South Pole Station in winter, from data in Figure 4b of *Walden et al.* [2003]. Also shown are lognormal fits corresponding to columns and plates: Γ_{mode} = 0.45 and 3.2, and σ_g = 0.18 and 0.34.

Figure 12a confirms the desired result for reflectance at $\lambda = 0.5$ μm, in that the error is small for all cases where $R \approx 1$ regardless of cloud optical depth. Results for $\lambda = 1.6$ μm are displayed in Figures 12b–12d. There, minima in reflectance and absorptance errors correspond to $R \approx 0.9$, while the minimum in transmittance error corresponds to $R \approx 1.1$. We conclude that for a similarity parameter ratio in the range 0.9–1.0, the minimum error is about 0.04, and a value of $R = 1$ predicts errors in r, t, and a of at most ±0.06 at both wavelengths. Although not discriminated in the figure, a point-by-point analysis of the pattern of errors reveals that the largest errors correspond to optical depths $\tau \approx 1$, while very thick and very thin clouds lead to small errors regardless of the value of R. These observations are consistent with the error results displayed in Figures 6–9. We conclude that $R \approx 1$ is a sufficient condition for agreement at about the 0.06 level.

[34] In geometric optics, Q_{ext} for the crystals is taken to be identically equal to 2 while for the spheres the precise value is slightly larger for the cases considered here. This produces a slight bias in the ratio of optical depths of the two media as is evident from equation (18). Correcting for this would shift the R value for minimum predicted error from 1.0 to 0.97 and 0.95 for $\lambda = 0.5$ μm and 1.6 μm respectively. Since we do not know the exact values of Q_{ext} for the crystals, however, we cannot make an accurate correction here and simply point out that the slight bias is consistent with the results in Figure 12.

5.1. Similarity Ratios for a Distribution Over Aspect Ratio

[35] Next we would like to test whether the effective similarity ratio R_{eff}, using F_{eff} from equation (22) together with the effective values of $\omega_{o,x}$ and g_x, has a predictive accuracy for using equal-V/A spheres for a distribution over particle shapes comparable to the results for individual particles. We have calculated the R_{eff} values for the South

Pole particle distributions over aspect ratio (Figure 10) using the following generalization of equation (16):

$$R_{eff} = F_{eff} \frac{(1 - g_s) \, \omega_{o,s}}{(1 - g_{x\_eff}) \, \omega_{o,x\_eff}}, \qquad (26)$$

where

$$\omega_{o,x\_eff} = \frac{\int_{\Gamma_{min}}^{\Gamma_{max}} \omega_{o,x} \, Q_{ext,x}(\Gamma) \langle P(\Gamma) \rangle \, N(\Gamma) \, d\Gamma}{\int_{\Gamma_{min}}^{\Gamma_{max}} Q_{ext,x}(\Gamma) \langle P(\Gamma) \rangle \, N(\Gamma) \, d\Gamma} \qquad (27)$$

$$g_{x,eff} = \frac{\int_{\Gamma_{min}}^{\Gamma_{max}} g_x \, \omega_{o,x} \, Q_{ext,x}(\Gamma) \langle P(\Gamma) \rangle \, N(\Gamma) \, d\Gamma}{\int_{\Gamma_{min}}^{\Gamma_{max}} \omega_{o,x} \, Q_{ext,x}(\Gamma) \langle P(\Gamma) \rangle \, N(\Gamma) \, d\Gamma}. \qquad (28)$$

[36] Calculations of R_{eff} were carried out separately for the plate mode ($\Gamma_{\text{mean}} < 1$), for the column mode ($\Gamma_{\text{mean}} > 1$), and for the entire distribution, and then compared with the corresponding maximum errors in reflectance (Figure 13). The values of R_{eff} range from 0.64 to just above 2.0, while the maximum reflectance error ranges from about −0.1 to +0.13 in a narrow envelope similar to the envelope of Figures 12a and 12b. Errors are positive for the columns, negative for the plates, and span the envelope. The envelope crosses the zero error line at $R_{\text{eff}} \approx 0.9$, similar to Figure 12.

5.2. Geometric Considerations

[37] The use of equal-V/A spheres implies a reclassification of some scattering events from "single scattering" to "multiple scattering." Scattering from the inside surfaces of particles with concavities adds complexity to the single scattering parameters and in some cases involves rays exiting and reentering the same particle. With equal-V/A spheres, this extra scattering is taken into account by requiring more and smaller spheres (Figure 2) and by enhancing the multiple scattering. The diameter of the spheres tends to match the thickness of the walls of the hollow crystals, so that for a given particle mass, increased fluffiness translates into more smaller spheres. The enhancement of multiple scattering is accomplished by adjusting the ratio of optical depth of the clouds of spheres to that of the crystals appropriately for the radiative transfer calculations using equation (18).

[38] Equal-V/A spheres may provide a useful way of describing the radiative effects of complex cloud particles from remote sensing observations. The description identifies the appropriate effective size scale for scattering without requiring a precise knowledge of the geometry of the crystals involved.

6. Conclusions

[39] For single scattering at wavelengths 0.5 and 1.6 μm, where the largest discrepancies occurred in our previous
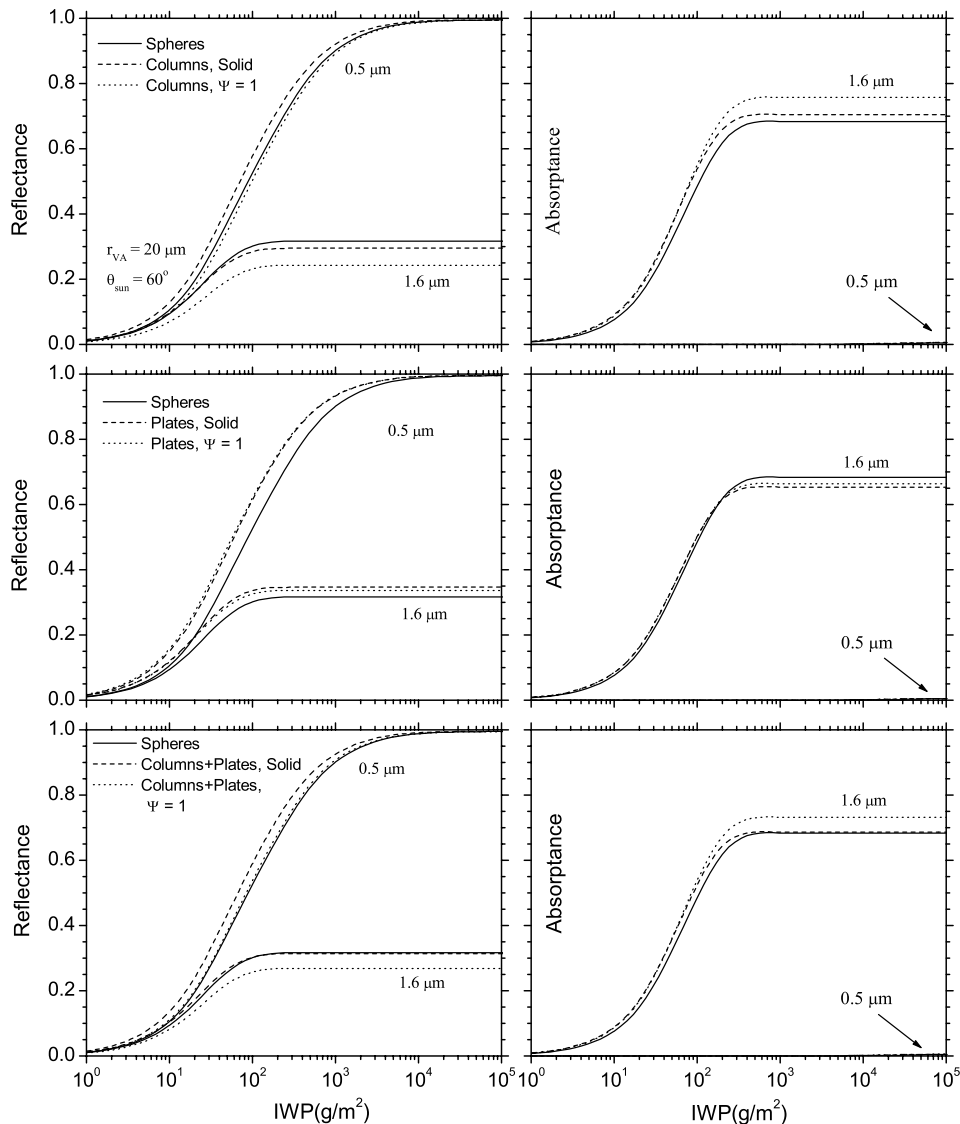
Figure 11. Reflectance and absorptance at wavelengths 0.5 and 1.6 μm, as functions of ice-water path (IWP) for clouds of equivalent spheres, and for clouds of crystals with $\Psi = 0$ and $\Psi = 1$ with the Γ-distribution functions shown in Figure 10, for $r_{VA} = 20$ μm and solar zenith angle 60°. (a, b) Columns. (c, d) Plates. (e, f) Columns and plates. Absorptance is very small at $\lambda = 0.5$ μm (arrows).

analysis, the accuracy provided by equal-V/A spheres depends on asymmetry parameter and degree of hollowing. For the cases considered here, errors in single-scattering coalbedo at $\lambda = 1.6$ μm are small, with $[\Delta(1 - \omega_o)]/(1 - \omega_o)$ less than 5%. At $\lambda = 0.5$ μm the absorption is so weak that errors in ω_o have no effect on multiple-scattering results. Asymmetry parameters vary significantly with Γ, even holding r_{VA} constant. We show, however, that the most relevant criterion for comparison is not just the value of g, but instead the similarity ratio R (equation (16)) based on the quantity $(1 - g)\omega_o/F$, where F is the "fluffiness" of the crystals.

[40] The errors in fluxes introduced by equivalent spheres are largest near $\tau \sim 1$, but the use of the similarity ratio and choosing configurations for which $R \sim 1$ does identify the situations where the error is small. In addition, the errors are small for large and small optical depths, thus $R \sim 1$ is

sufficient although not necessary for identifying good agreement. For the distribution of aspect ratios found by *Walden et al.* [2003], reflectance and absorptance are matched by the equivalent-sphere model at all optical depths, with maximum errors of about 0.08.

[41] Our earlier work [*Neshyba et al.*, 2003] showed significant multiple-scattering errors in the equivalent-sphere representation for certain ranges of aspect ratios for solid plates and columns. The errors were explained by phenomena of direct transmission through plates and corner-reflection by equidimensional prisms, so we speculated that the multiple-scattering errors would be smaller for the irregular crystals typical of natural clouds. That speculation has not been borne out by the current study, which found errors for hollow prisms comparable to and sometimes exceeding those for solid prisms. However, there is more to be investigated; the irregularity in natural crystals still
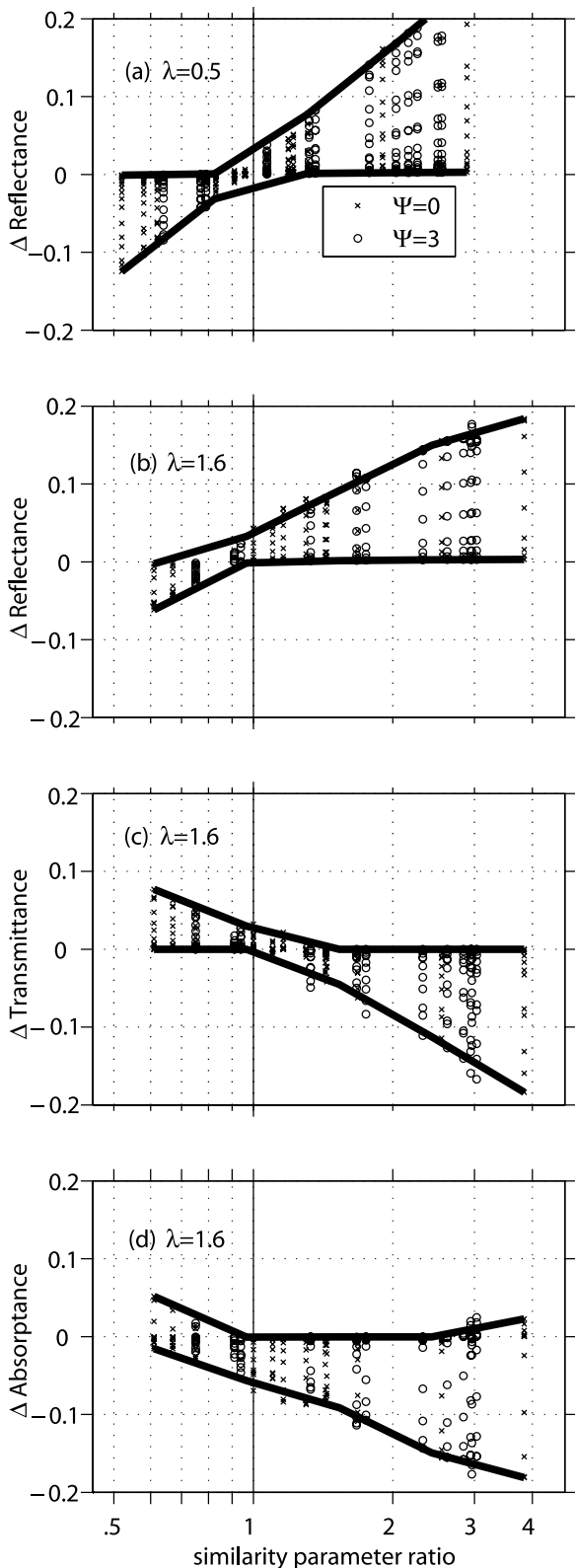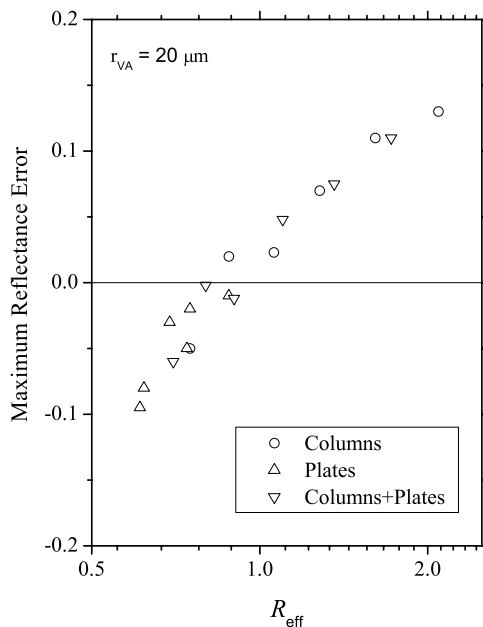
Figure 13. Maximum error in reflectance, versus R_{eff}, for columns, plates, and plates plus columns for the frequency distributions presented in Figure 10, with $r_{VA} = 20$ μm.

greatly exceeds the ideal shapes studied here. As *Walden et al.* [2003] showed, the internal walls of hollow bullets are not flat but rather corrugated. Asymmetry parameters for crystals sampled in Arctic clouds have $g_x \approx 0.74$, smaller than any of the crystals studied here (Figure 4). Since $g_s \approx 0.87$ for the equal-*V/A* spheres, in that case the enhanced optical depth from fluffiness would counteract the difference in g, unlike in the cases studied in this paper. This suggests that the equivalent-sphere representation will work better for the more irregular crystals found in real clouds than for the ideal shapes we have studied thus far.

[42] We conclude that the method of equal-*V/A* spheres can be used for hexagonal columns and plates, both solid and hollow, provided the error plots are consulted for the crystal shapes and optical depths of interest. The formulation developed in this paper for representing hollow crystals as equal-*V/A* spheres can also be applied to more complex crystal shapes such as bullet rosettes, irregular shapes and complex clusters, that often occur in cirrus clouds. Its accuracy for such complex shapes remains to be determined.

References

Coakley, J. A., Jr., and P. Chylek (1975), The two-stream approximation in radiative transfer: Including the angle of the incident radiation, *J. Atmos. Sci.*, *32*, 409–418.

Gerber, H., Y. Takano, T. J. Garrett, and P. V. Hobbs (2000), Nephelometer measurements of the asymmetry parameter, volume extinction coefficient, and backscatter ratio in Arctic clouds, *J. Atmos. Sci.*, *57*, 3021–3034.

Grenfell, T. C. (1991), A radiative transfer model for sea ice with vertical structure variations, *J. Geophys. Res.*, *96*, 16,991–17,001.

Grenfell, T. C., and S. G. Warren (1999), Representation of a nonspherical ice particle by a collection of independent spheres for scattering and absorption of radiation, *J. Geophys. Res.*, *104*(D24), 31,697–31,709.

Figure 12. Calculated errors (sphere-crystal) in reflectance, transmittance, and absorptance at λ = 0.5 and 1.6 μm, as functions of the similarity parameter ratio, for a solid hexagon (Ψ = 0) and for a tapered hollow hexagon (Ψ = 3), both with r_{VA} = 20 μm. At 0.5 μm the absorptance is negligible, so we show only the reflectance error.

Havemann, S., and A. J. Baran (2001), Extension of T-matrix to scattering of electromagnetic plane waves by non-axisymmetric dielectric particles: application to hexagonal ice cylinders, *J. Quant. Spectrosc. Radiat. Transfer*, *70*, 139–158.

Heymsfield, A. (1975), Cirrus uncinus generating cells and the evolution of cirriform clouds: Part I. Aircraft observations of the growth of the ice phase, *J. Atmos. Sci.*, *32*, 799–808.

Liou, K. N. (2000), *An Introduction to Atmospheric Radiation*, 2nd ed., Elsevier, New York.

Macke, A., J. Mueller, and E. Raschke (1996), Single scattering properties of atmospheric ice crystals, *J. Atmos. Sci.*, *53*, 2813–2825.

Mishchenko, M. I., L. D. Travis, and A. A. Lacis (2002), *Scattering, Absorption, and Emission of Light by Small Particles*, Cambridge Univ. Press, New York.

Neshyba, S. P., T. C. Grenfell, and S. G. Warren (2003), Representation of a nonspherical ice particle by a collection of independent spheres for scattering and absorption of radiation: 2. Hexagonal columns and plates, *J. Geophys. Res.*, *108*(D15), 4448, doi:10.1029/2002JD003302.

Ono, A. (1969), The shape and riming properties of ice crystals in natural clouds, *J. Atmos. Sci.*, *26*, 138–147.

Schmitt, C. G., and A. J. Heymsfield (2005), Total surface area estimates for individual ice particles and particle populations, *J. Appl. Meteorol.*, *44*, 467–474.

van de Hulst, H. C. (1980), *Multiple Light Scattering: Tables, Formulas, and Applications*, vol. 2, Elsevier, New York.

Vouk, V. (1948), Projected area of convex bodies, *Nature*, *162*, 330–331.

Walden, V. P., S. G. Warren, and E. Tuttle (2003), Atmospheric ice crystals over the Antarctic Plateau in winter, *J. Appl. Meteorol.*, *42*, 1391–1405.

Wiscombe, W. J. (1979), Mie scattering calculations: Advances in technique and fast, vector-speed computer codes, *NCAR Tech. Note TN-140+STR*, Natl. Cent. for Atmos. Res., Boulder, Colo.

Wiscombe, W. J. (1980), Improved Mie scattering algorithms, *Appl. Opt.*, *19*, 1505–1509.

Yang, P., and K. N. Liou (1996), Finite-difference time domain method for light scattering by small ice crystals in three-dimensional space, *J. Opt. Soc. Am. A Opt. Image Sci.*, *13*(10), 2072–2085.

Yang, P., and K. N. Liou (1997), Light scattering by hexagonal ice crystals: Solutions by a ray-by-ray integration algorithm, *J. Opt. Soc. Am. A Opt. Image Sci.*, *14*(9), 2278–2289.

_____

T. C. Grenfell and S. G. Warren, Department of Atmospheric Sciences, Box 351640, University of Washington, Seattle, WA 98195-1640, USA. (tcg@atmos.washington.edu; sgw@atmos.washington.edu)

S. P. Neshyba, Department of Chemistry, University of Puget Sound, 1500 North Warner, Tacoma, WA 98416, USA. (nesh@ups.edu)